lubricants

Article

The Verification of Engine Analysis Model Accuracy by Measuring Oil Film Pressure in the Main Bearings of a Motorcycle High-Speed Engine Using a Thin-Film Sensor

Takumi Iwata [1,*], Masakuni Oikawa [2], Michiyasu Owashi [3], Yuji Mihara [2], Keisuke Ito [4], Yoshinari Ninomiya [4], Yohei Kato [4] and Shinya Kubota [4]

1 Mechanics, Tokyo City University Graduate School, 1-28-1, Tamazutsumi, Setagaya-ku, Tokyo 158-8557, Japan
2 Department of Mechanical Engineering, Tokyo City University, 1-28-1, Tamazutsumi, Setagaya-ku, Tokyo 158-8557, Japan
3 Sustainable Engine Research Center Co., Ltd., 1-33, Yayoicho, Inage-ku, Chaba-shi, Chiba 263-8522, Japan
4 Motorcycle Engineering Department, Suzuki Motor Co., 8686, Miyakoda-cho, Kita-ku, Hamamatsu-shi, Shizuoka 431-2102, Japan
* Correspondence: g2291001@tcu.ac.jp; Tel.: +81-3-5707-2100

Abstract: To improve the accuracy of the calculation analysis of crank journal bearings in motorcycle engines and accurately understand lubrication conditions, the oil film conditions of actual crankshafts and journal bearings should be measured. This research study focuses on the oil film pressure generated in the main bearing, and by using an original thin-film pressure sensor with improved durability achieved through the use of DLC (Diamond-like Carbon), it was possible to perform experiments at a maximum of 13,000 rpm and full load, which was not possible before. This established a method for measuring the oil film pressure generated in the main bearing of a high-speed motorcycle engine during operation without changing the surrounding environment. The maximum oil film pressure was 140 MPa, and the oil film pressure generated by each main bearing was successfully measured under different experimental conditions. The timing of pressure onset agreed well between the calculation and experiment stages, but the peak oil film pressure values were different. By varying the temperature of the engine in the calculation model, the calculated values approached the measured values. In the future, we plan to investigate ways to improve the accuracy of the current analytical model.

Keywords: heat engine; engine component or element; plain bearing; thin-film sensor; oil film pressure; EHL; MBD

Citation: Iwata, T.; Oikawa, M.; Owashi, M.; Mihara, Y.; Ito, K.; Ninomiya, Y.; Kato, Y.; Kubota, S. The Verification of Engine Analysis Model Accuracy by Measuring Oil Film Pressure in the Main Bearings of a Motorcycle High-Speed Engine Using a Thin-Film Sensor. *Lubricants* **2022**, *10*, 314. https://doi.org/10.3390/lubricants10110314

Received: 13 October 2022
Accepted: 15 November 2022
Published: 18 November 2022

1. Background and Purpose

Further improvements in the fuel economy have been required when developing new engines in recent years with the aim of achieving a carbon-neutral society. To meet this requirement, engines are being downsized and their weights are reduced, among other improvements. Consequently, it can be expected that sliding engine parts will experience more severe lubrication conditions due to increased surface pressure and lower rigidity. Such conditions can heighten the risk that the main bearings will suffer greater wear or seizure.

Model-based development (MBD) is vigorously being used in engine development work today, but one issue of concern here is the correlation between simulation results and experimental data. A large motorcycle engine that was the subject of this study must be able to operate under a wide range of conditions up to high engine speeds and loads. The application of a simulation model requires better simulation accuracy for a broad range of phenomena that occur under such operating conditions. The oil film pressure that develops on the sliding surfaces of the crankshaft and main bearings in particular is affected by inertial forces and combustion pressures occurring among the cylinders. Because the phenomena involved are particularly complex, it is indispensable to improve calculation accuracy based on actual measurements.

Previously, hydrodynamic pressure measurements were obtained using piezoelectric or diaphragm-type pressure sensors, which were cylindrical or button-shaped [1–4]. One problem with using these sensors is that the measurement environment changes when the sensor is attached to a part, e.g., leading to a reduction in the rigidity of the part. A thin-film pressure sensor with a thickness of 2 to 6 μm was developed mainly for measuring the rolling contact pressure of two cylinders, and was mainly used to verify elastohydrodynamic lubrication (EHL) simulations [5]. After that, the contact pressure between the inner ring and the roller of the cylindrical roller bearing was measured and the tooth flank of the gear was applied. On the other hand, there was one case of application to a plain bearing in a single-cylinder engine [6]; however, it was difficult to apply it to multi-cylinder engines because it required the journal parts of the engine to be significantly modified. In addition, in experiments using thin-film sensors, the thin-film sensor was not sufficiently guaranteed when the machine element part was deformed by the applied bearing load.

In 2002, Mihara et al. [7] developed special-shaped thin-film sensors fabricated by a sputtering method to measure the oil film pressure on the main bearing surface of a test engine (5300 cm^3 in-line four-cylinder turbo-charged diesel engine) during the actual operation for the first time. They measured the overall lubrication state on the surface of plain bearings at every crank angle. In addition, two semi-arc-type thin-film sensors were developed to significantly reduce pressure measurement errors caused by plain bearing strain by deformation during the engine operation. Furthermore, on the sliding surfaces of internal combustion engines, instantaneous changes in surface temperature caused pressure measurement errors, so the composition ratio of the pressure-sensing alloys (Cu, Mn, and Ni) for the thin-film sensor was optimized to achieve high measurement accuracy. The results of a comparison of the measured and calculated oil film pressures of the main bearing by applying these techniques were reported in 2007 [8]. The results of actual measurements of the oil film pressure on the piston skirt, piston ring, piston pin boss, spur gear, and helical gear tooth flanks have also been reported previously [9–13]. Subsequently, by 2017, a multilayer sensor with two alloy layers of sensor film was developed to reduce the pressure measurement error due to strain to zero [9].

Recent examples of the use of thin-film sensors, other than in the engine's sliding parts, include temperature measurements under EHL lubrication and without lubrication in an FZG twin-disk test rig [14,15] and oil film pressure measurements in a CVT (Continuously Variable Transmission) pulley [16]. However, there are no reports of measurements of oil film pressure on the surface of main bearings in engines under high speed and high load conditions. This is because thin-film sensors have a high risk of disconnection when the plain bearing part is in a mixed or boundary lubrication region. There is a need to improve sensor durability under such conditions so as to minimize the risk of sensor damage. Accordingly, as the first step in the present work, thin-film sensors were fabricated on the main bearing surface of a motorcycle engine in the process of improving the fabrication and measurement methods so as to enable oil film pressure measurement under high speed and high load conditions. In particular, to improve the durability of thin-film sensors, we focused on DLC, which has high wear resistance [17–22]. Oil film pressures measured under actual engine operation were also compared with simulation results for the purpose of improving calculation accuracy.

2. Experimental Conditions

2.1. Test Engine

This study was conducted using an in-line, 4-cylinder, 4-stroke, water-cooled gasoline engine (Suzuki Motor Co., Hamamatsu, Japan) with a displacement of 999 cm^3. The main engine specifications are shown in Table 1. The bore was 76.0 mm, and the stroke was

55.0 mm. The motorcycle engine oil of the 10W-40 SAE viscosity grade was used as the lubrication oil.

Table 1. Test engine specifications.

Item	Specification
Engine type	Water-cooled DOHC 4-stroke 16 valves In-line 4-cylinder gasoline engine
Bore / stroke (mm)	76.0/55.1
Displacement (cm^3)	999
Compression ratio	13.2:1
Max. power (kW/(r/min))	145/13,200
Max. torque (N·m/(r/min))	117/10,800

2.2. Confirmation of Main Bearing Cross-Sectional Shape after Running-In Operation

It is important to confirm the main bearing cross-sectional shapes after running-in operations in order to fabricate thin-film sensors on the main bearing surface in order to accurately measure the oil film pressure. In many cases, the wear shown in Figure 1 is found at the ends of plain bearings after running-in operations, owing to the effects of oil film pressure and accompanying elastic deformation of the bearings. The oil film pressure distribution to be measured in this study involved the oil film generation state at the crank journal after the initial crank journal running-in operations were completed. Therefore, thin-film sensors were formed along the bearing geometry after running-in operations. In addition, forming the thin-film sensor in the shape after running-in operations reduced direct contact with the sensor during measurement process and improved the durability of the sensor.

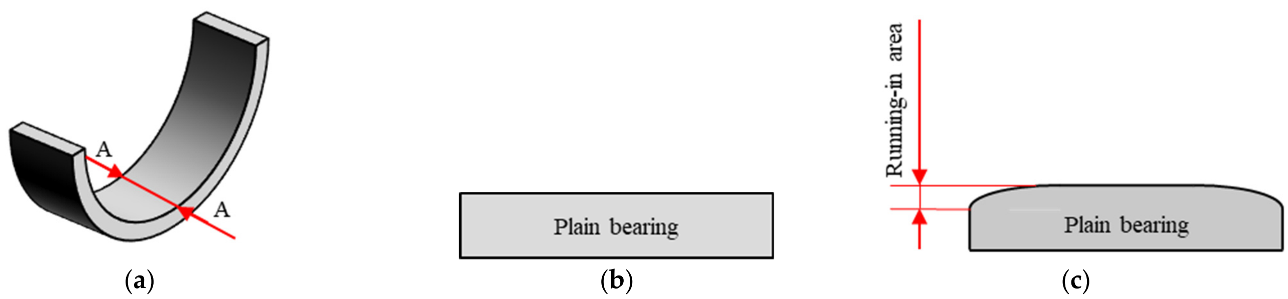

Figure 1. Cross-sectional view of plain bearing: (**a**) external view of plain bearing; (**b**) initial cross-section of A-A; (**c**) after running-in.

3. Thin-film Pressure Sensor

3.1. Measurement Principle

A thin-film pressure sensor is an alloy film resistor with an electrical resistance of around 120–500 Ω, which varies according to changes in pressure. Using a Wheatstone bridge circuit, changes in the electrical resistance were converted to changes in the voltage and were recorded, as shown in Figure 2. Resistance changes due to pressure changes are mainly caused by changes in electrical resistivity, but since the basic measurement principle is the same as that of strain gauges, large changes in strain or temperature can cause pressure measurement errors. Therefore, it was important to minimize the sensitivity of the sensor to strain and temperature.

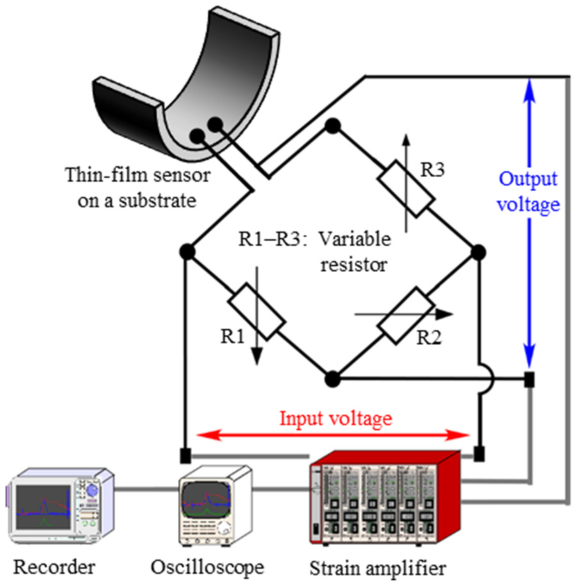

Figure 2. Measurement system for thin-film sensors.

3.2. Fabrication Procedure

Thin-film sensors were deposited using the sputtering equipment shown in Figure 3. A thin film was deposited on a bearing from the sliding surface to the side surface of the end face (see Figure 9b). For this purpose, the main bearing ④ was attached to a substrate holder ③ that is rotated by a motor ② inside a vacuum chamber ①. The bearing was rotated at 3 rpm so that its sliding surface and end face were periodically opposite the film deposition material (target) ⑤. This enabled thin-film fabrication up to the end face of the bearing. As will be described in Section 3.6, lead wires were formed from the side of the bearing end face. A uniform thin film was successfully fabricated by rotating the bearing inside the sputtering apparatus.

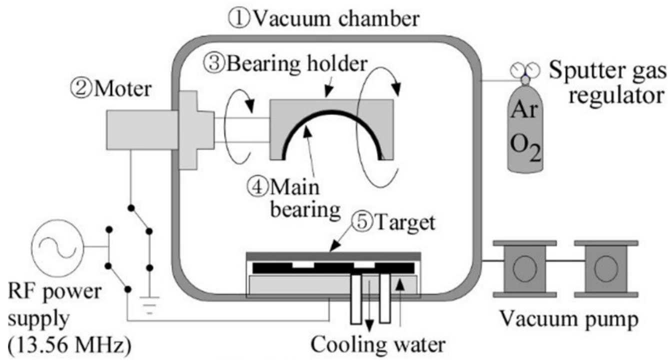

Figure 3. Sputtering equipment.

3.3. Sensor Structure

Figure 4a shows the basic structure of a thin-film pressure sensor for the main (plain) bearings. An Al_2O_3 insulating film ② was formed on the surface of the substrate ① to maintain insulation between the substrate and the pressure sensor alloy film ③. A Cu-Mn-Ni sensor film ③ used for sensing pressure was sputtered on this insulating film using a photoresist method. In addition, a protective film was formed to improve the sensor durability due to contact with the journal shaft surface facing the sensor film, and the total film thickness was 5.2 μm. The protective film ④ was changed from the previous Al_2O_3 film to a diamond-like carbon (DLC) coating to improve sensor durability. If the oil clearance between the journal and bearing varied from the engine standard due to sensor formation, the oil film pressure may be affected. Therefore, the thickness of the bearing used for sensor formation was reduced by the total thickness of the thin-film sensor, and the thickness after sensor formation was aligned with the engine standard. The photos in Figure 5 show the appearance of the main bearings following the deposition of the DLC protective film. Any sensor film is applied only to the plain bearing surfaces and end faces, and not to the rear surface of the bearing due to optimal masking techniques. Therefore, even if the bearing with sensor is installed in the engine, the oil clearance will not change.

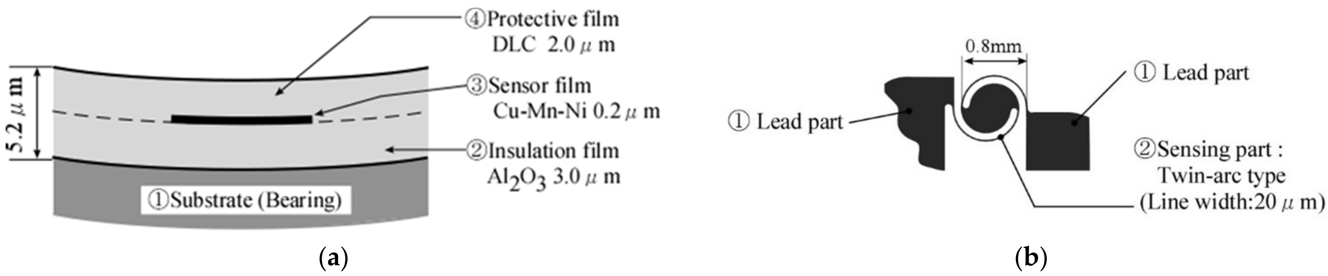

Figure 4. Structure and geometry of thin-film sensor: (**a**) structure of thin-film sensor; (**b**) sensor form.

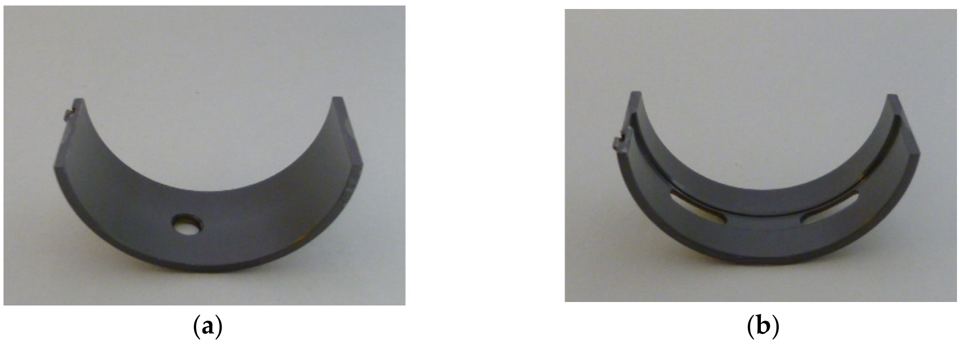

Figure 5. Main bearing after DLC protective film deposition: (**a**) bearing ♯1, ♯3, and ♯5; (**b**) bearing ♯2 and ♯4.

3.4. Sensor Film Shape

As shown in Figure 4b, the sensor consisted of a lead part ① for leading the pressure signal and a pressure sensing part ②. The pressure sensing part was 0.8 mm in diameter and had a line width of 20 μm; it was fabricated in the shape of two arcs that were connected in the center of the two semi-circle shapes. This original sensor shape was selected to minimize the gauge factor of the thin-film pressure sensor [7].

3.5. Measurement Positions

Figure 6 shows the cylinder numbers and main bearing numbers of the engine used in the experiment. Cylinder numbering is the 1st, 2nd, 3rd, and 4th from the front side of the engine, and the main bearings are also #1, #2, #3, #4, and #5 from the front side. Figure 7 shows the calculated results of the pressure applied to the lower side of each main bearing. All of them show the highest pressure at around the 180-degree position in Figure 7 and are assumed to be under severe lubrication conditions. Figure 8 shows the measurement position of the lower-side main bearings. Based on the calculation results in Figure 7, for main bearings #1, #3, and #5, the position of the sensing part was set at the center position in the bearing width and 5.2 mm from the center to the front and rear side of the engine, respectively (Figure 8a). In main bearings #2 and #4, the measurement position was set to 5.2 mm from the center of the bearing to the front and rear side, respectively, due to the effect of the oil feed groove (Figure 8b). Among all the data measured by these sensors, the sensors with reliable data were selected and the experimental results were summarized in Chapter 5.

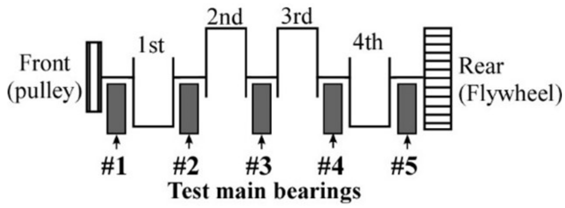

Figure 6. Cylinder number and main bearing number.

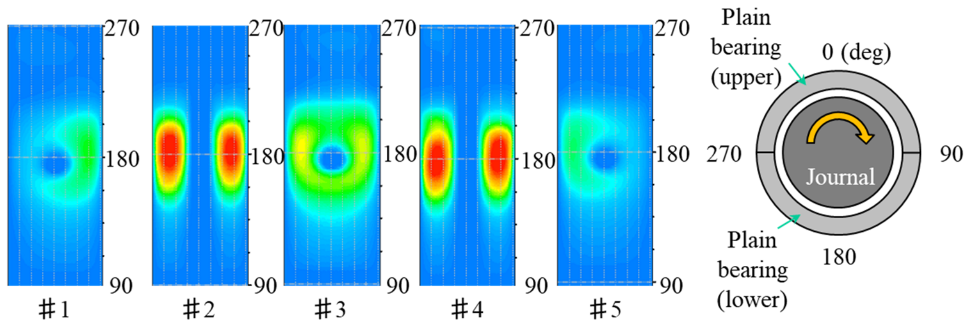

Figure 7. Calculated pressure results on lower plain bearing surface.

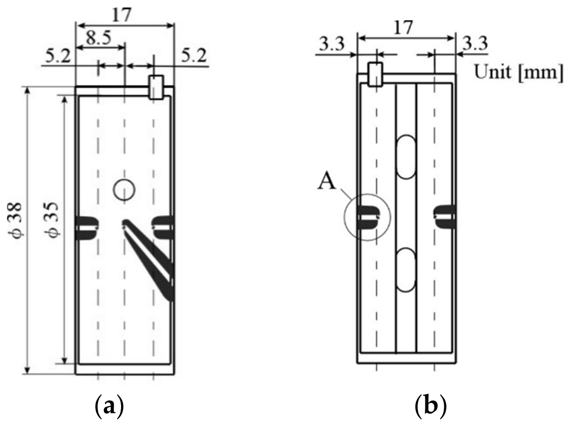

Figure 8. Measurement position of thin-film sensor: (**a**) sensor location (♯1,3,5); (**b**) sensor location (♯2,4).

3.6. Wiring for Taking Sensor Signal out from the Engine

Figure 9a shows a side view of the main bearing after thin-film sensor formation. As shown in Figure 9b, the lead part ① was sputtered as far as the side surface of the bearing end face in order to take the thin-film sensor signal out via a lead wire and avoid contact with the crankshaft. A wire ② 50 μm in diameter was welded to the side surface of the lead part ① and connected to an external Cu lead wire ④ via a terminal ③. The external Cu lead wire ④ was connected via the housing wall surface to measure instruments located outside the engine. In this way, oil film pressure measurements were obtained without doing any machining that would change the rigidity or shape of the bearings and the bearing housing. As described in 3.5, in this chapter, among the thin-film sensors attached to slide bearings #1 to #5, the measurement data of sensors with high experimental data accuracy were used. For this reason, data from 9 of the 13 measurement points shown in Figure 8 were used and summarized. These sensor positions are shown in Table 2.

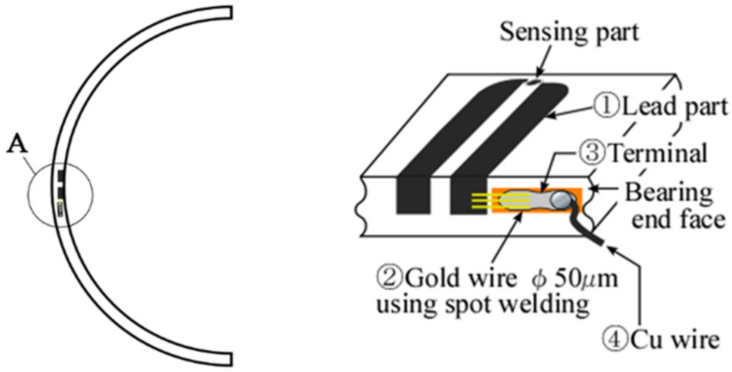

(**a**) (**b**)

Figure 9. Wiring from thin-film sensor: (**a**) side view of main bearing after thin-film sensor formation; (**b**) detail of end face of A.

Table 2. Symbols of sensors on main bearings used as experimental data in this study.

Main Bearing No.	Sensor Location
1	♯1-C ♯1-R
2	♯2-R
3	♯3-C ♯3-R
4	♯4-F ♯4-R
5	♯5-C ♯5-R

3.7. Calibration Results for Pressure Sensitivity

Figure 10 shows the results of a pressure sensitivity calibration for the thin-film pressure sensor in a pressure range of 0–50 MPa. As shown in Figure 10a, a bearing deposited with a thin-film pressure sensor was placed in a pressure vessel that was pressurized to 50 Mpa using a high-pressure oil pump in order to determine the calibration values. The results plotted in Figure 10b indicate that the pressure sensitivity of the thin-film sensor was approximately 9 $\mu\varepsilon$/Mpa. It was determined that measurement errors, due to the temperature and strain sensitivities of the thin-film pressure sensor, were negligibly small after optimizing the sensor structure [7].

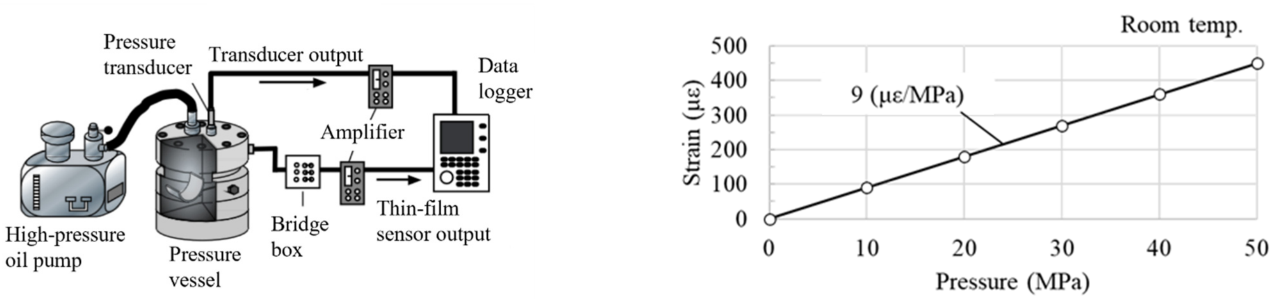

(**a**) (**b**)

Figure 10. Pressure sensitivity calibration: (**a**) calibration apparatus; (**b**) pressure sensitivity characteristics.

3.8. Measurement System

The measurement system used in this study is shown schematically in Figure 11. Bearings deposited with thin-film pressure sensors ② were installed in the lower crankcase ① of the test engine. A signal cable was connected to a bridge box ③ and a dynamic strain amplifier ④ was situated in a measurement room. An oscilloscope ⑤ and an AVL data acquisition system ⑥ were used as recording devices for combustion analysis. A ground wire was connected to the double-shielded signal cable running from right near the sensor-deposited bearings to the measurement instruments as a thorough measure for preventing noise in the oil film pressure measurements.

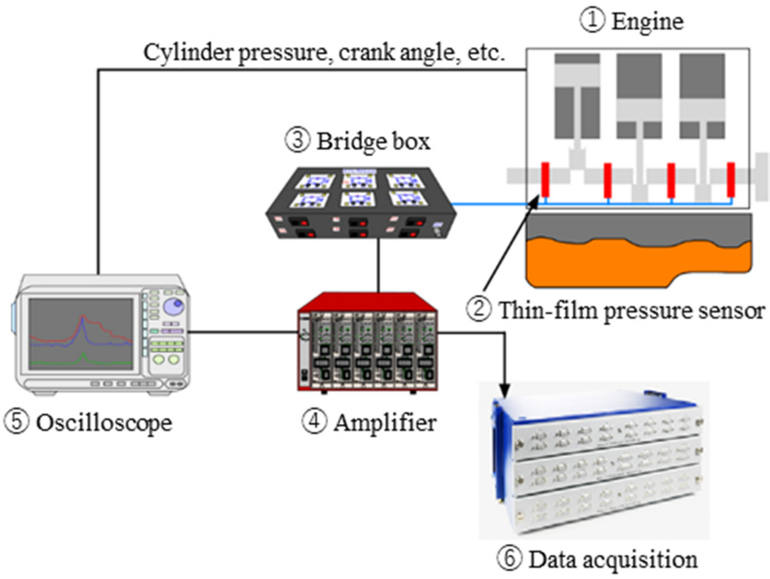

Figure 11. Measurement system.

4. Test Results

4.1. Measured Oil Film Pressure Results

Figure 12 shows the oil film pressure results at an engine speed of 5000 rpm and a load of 25%. The positions of the sensors and the symbols in Figure 12 are shown in Table 2. As a characteristic of the experimental results, a high peak of oil film pressure was measured at the bearing neighboring to the cylinder where the combustion pressure acts. For example, when the combustion pressure of the 4th cylinder was applied, #4-R was 122 MPa and #4-F was 86 MPa; however, #5-R was 5 MPa and #5-C was 15 MPa. It can be seen that the #4 bearing has a very large share of the bearing load due to the combustion pressure of the 4th cylinder (4th). Moreover, when the combustion pressure of the 1st cylinder (1st) was applied, #1-R in the #1 bearing obtained 65 MPa and #2-R obtained 75 MPa. From this result, the neighboring bearings showed almost the same load sharing. These tendencies are characteristic of the engine used in the experiment, and the inclination and deformation of the crank when a load is applied to each bearing, as well as the induced deformation of the main bearing, are considered to be the main causes of uneven load distribution.

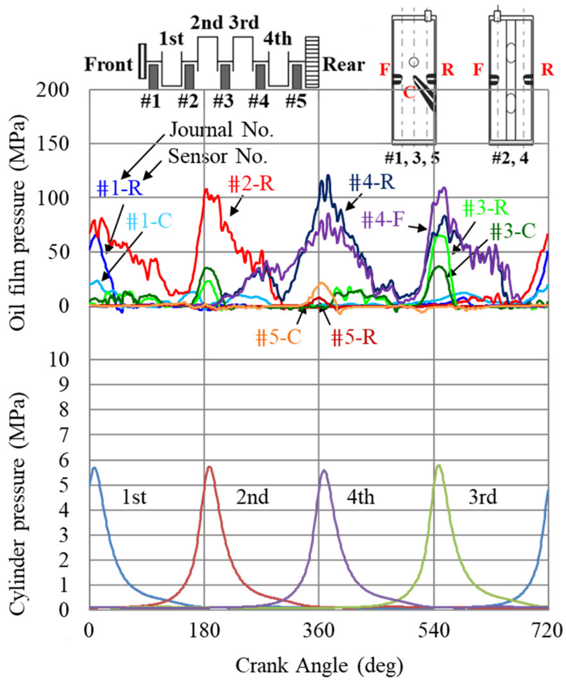

Figure 12. Measured oil film pressure results (oil temperature = 90 deg. C, engine speed = 5000 rpm, load = 25%),.

4.2. Measured Oil Film Pressure Results for Different Loads at 5000 rpm

Figure 13 shows the maximum oil film pressure at each measurement position under the three load conditions of 50% load and full load in addition to the 25% load at the rotation speed of 5000 rpm, as shown in Figure 12. At this rotational speed, #1-R and #3-R (right end of bearing) exceeded 60 MPa under all load conditions, and #1-C and #3-C (bearing center) fell below 40 MPa. It was understood that in these #1 and #3 bearings, an offset load was applied mainly to the right end of the bearing. It was found that #5-R and #5-C, which had the same geometry as these bearings, were lower than 20 MPa and the load distribution to the #5 bearing was low. In #2-R, #4-R, and #4-F, a high oil film pressure of 100 MPa to 120 MPa was generated at any load. As shown in Figure 8, the bearings of #2 and #4 had smaller sliding areas than those of #1, #3, and #5. For this reason, the surface pressure increased, which is considered to be the reason for the high oil film pressure.

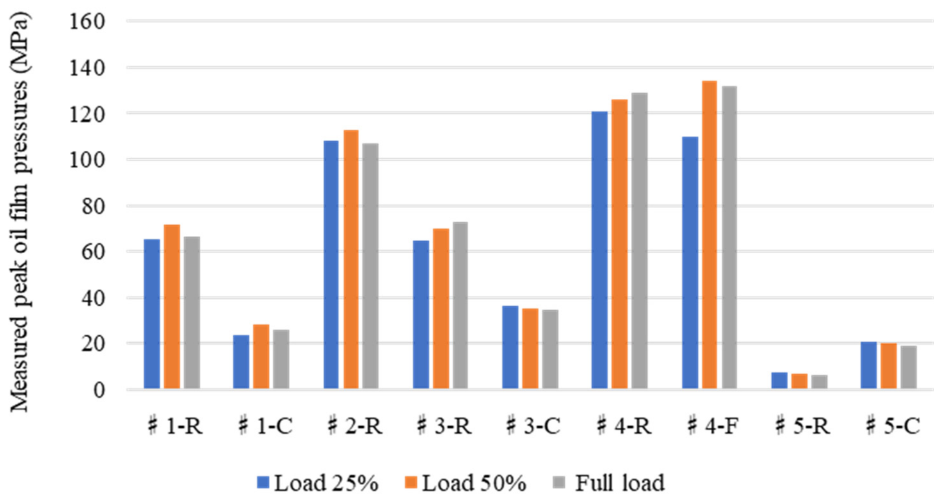

Figure 13. Measured peak oil film pressures (5000 rpm).

4.3. Measured Oil Film Pressure Results at Different Engine Speeds under Full Load Condition

Figure 14 shows the maximum oil film pressure at each measurement point when the load condition is full load and the rotation speed is changed to 5000 rpm, 10,000 rpm, and 13,000 rpm. The trend was similar to the results shown in Figure 13, but the oil film pressure at the #3-R and #3-C and #5-R and #5-C measurement points increased sharply when the rotation speed was 13,000 rpm, possibly due to an increase in inertial forces following an increase in the rotation speed. (Since the #4-F sensor lost its signal at 13,000 rpm, the measurement data were not recorded.)

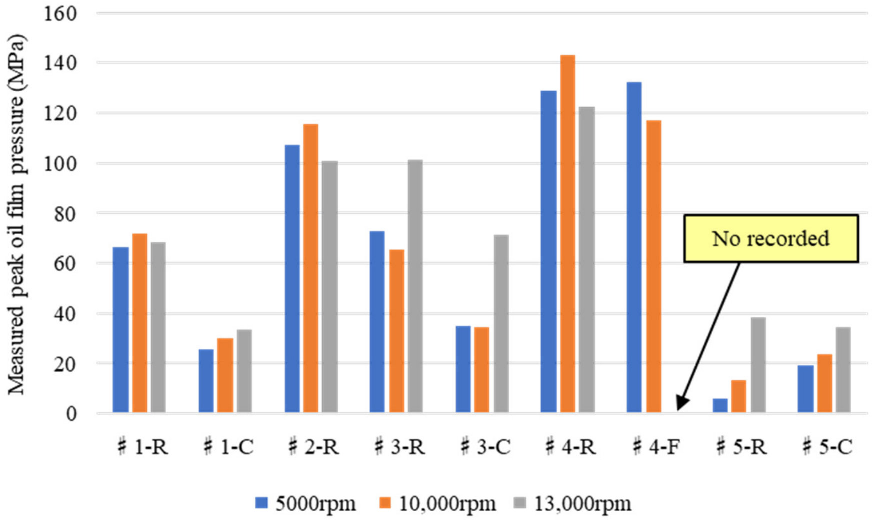

Figure 14. Measured peak oil film pressure (full load).

In addition, the generation of a peculiar oil film pressure was also measured by increasing the rotation speed. As an example of this phenomenon, Figure 15 shows the change in oil film pressure for each rotational speed at measurement position #1-R. At 5000 rpm, the oil film pressure rose to about 75 MPa in response to the increase in combustion pressure in the neighboring 1st cylinder. At 10,000 rpm and 13,000 rpm, the oil film pressure was almost the same at around 75 MPa when the combustion pressure of the 1st cylinder increased, but when the combustion pressure of the 2nd and 3rd cylinders acted, an increase in the oil film pressure ranging from 30 to 50 MPa was observed at the #1-R measurement point.

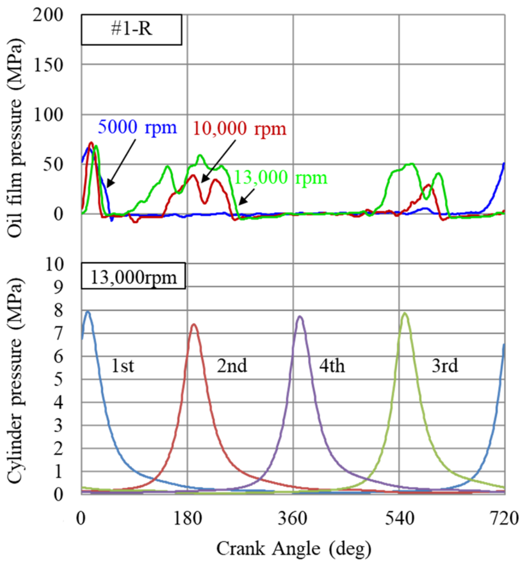

Figure 15. Change in oil film pressure at measurement position ♯1-R for different engine speeds.

5. EHL Simulation Results

5.1. Analysis Model

The software (AVL/EXCITE 2020) was used to perform elastohydrodynamic lubrication (EHL) simulations, and the calculated results were compared with the measured results for validation. The simulation model had the same structure as the engine used in the experimental measurements. A finite element (FE) model of the crankshaft and engine block (see Figure 16) was created, modeling only the mass of the pistons and connecting rods. Figure 17 is the 2D connection view of the simulation model. MB indicates main bearing, and EHD2 indicates the elastohydrodynamics joint. EHD2 joints calculate the modified Reynolds equation by a difference method. Cylinder pressure, engine speed, oil properties, oil supply conditions, bearing profile, and geometry are input parameters. In addition, the surface properties of the slide bearing and crankshaft journal used in this experiment were measured with a three-dimensional measuring instrument, and the results were entered into the simulation model as surface roughness, allowing the oil film pressure of each main bearing to be accurately calculated. The oil film pressure was calculated at the same location as the main bearing lower half measured on the test engine and compared with the measured results.

5.2. Comparison of Analysis Model and Experimental Results

Figure 18 compares the measured and calculated results under full load conditions and an engine speed of 5000 rpm. Figure 18a shows the oil film pressure of journal #1-R and Figure 18b shows the oil film pressure of journal #4-R. Looking at the results in Figure 18a, it can be seen that the oil film pressure of the #1-R journal increased as the cylinder pressure of the 1st cylinder increased. Both the calculated and measured results show that the oil film pressure reached its peak around 10 degrees ATDC (After top dead center). The peak pressure and calculated peak pressure were 66 MPa and 33 MPa, respectively, and the analytical value was about 50% smaller than the measured value.

Next, looking at the results in Figure 18b, the oil film pressure of the #4-R journal increased as the combustion pressure increased in the neighboring 4th and 3rd cylinders. Measured and calculated values reached maximum oil film pressure values at 375 and 555 degrees, respectively. Although there was a difference in the maximum value of the oil film pressure, almost the same result was obtained for the pressure generation timing at the crank angle.

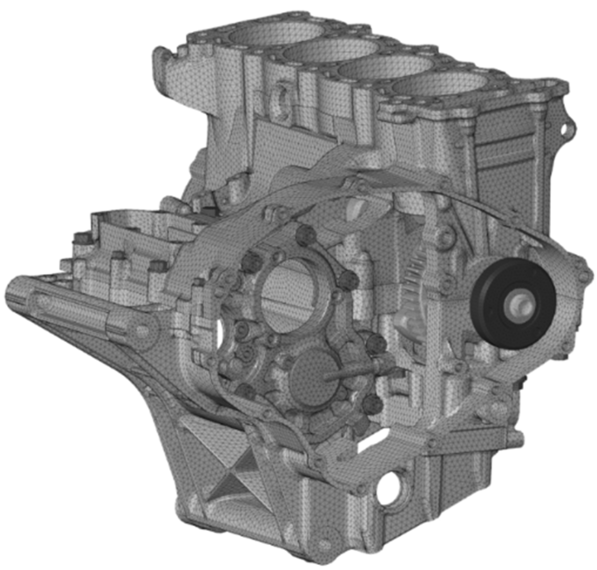

Figure 16. The FE engine model.

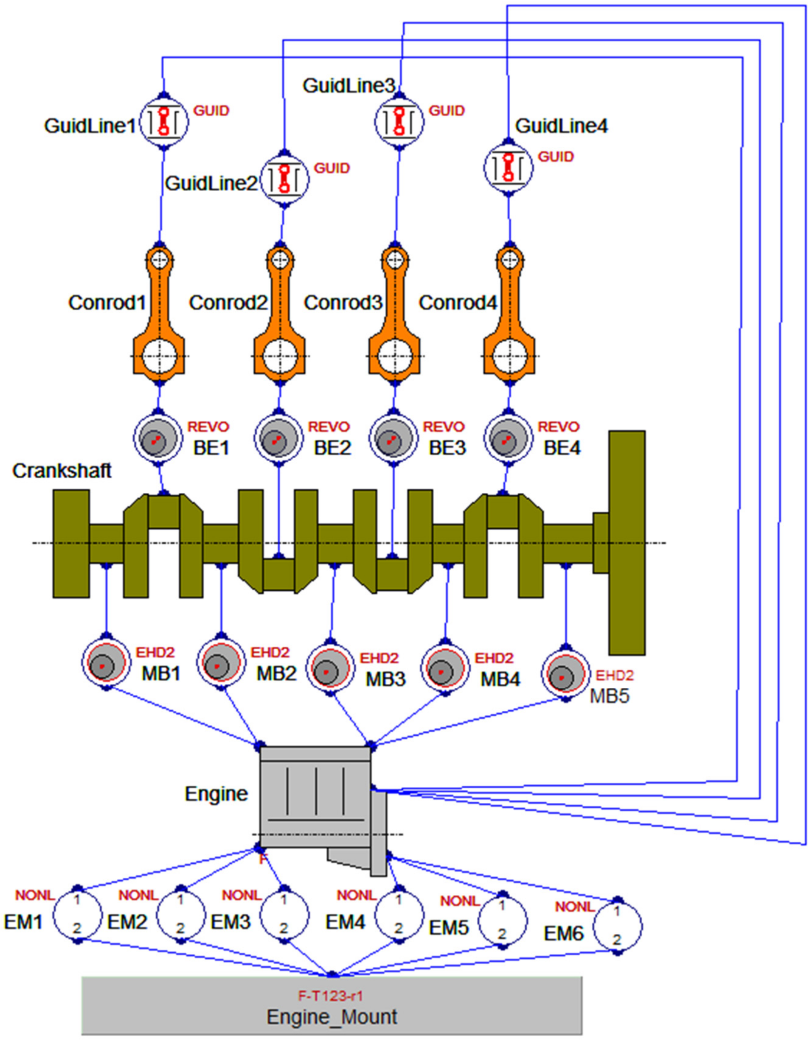

Figure 17. Two-dimensional connection view of the simulation model.

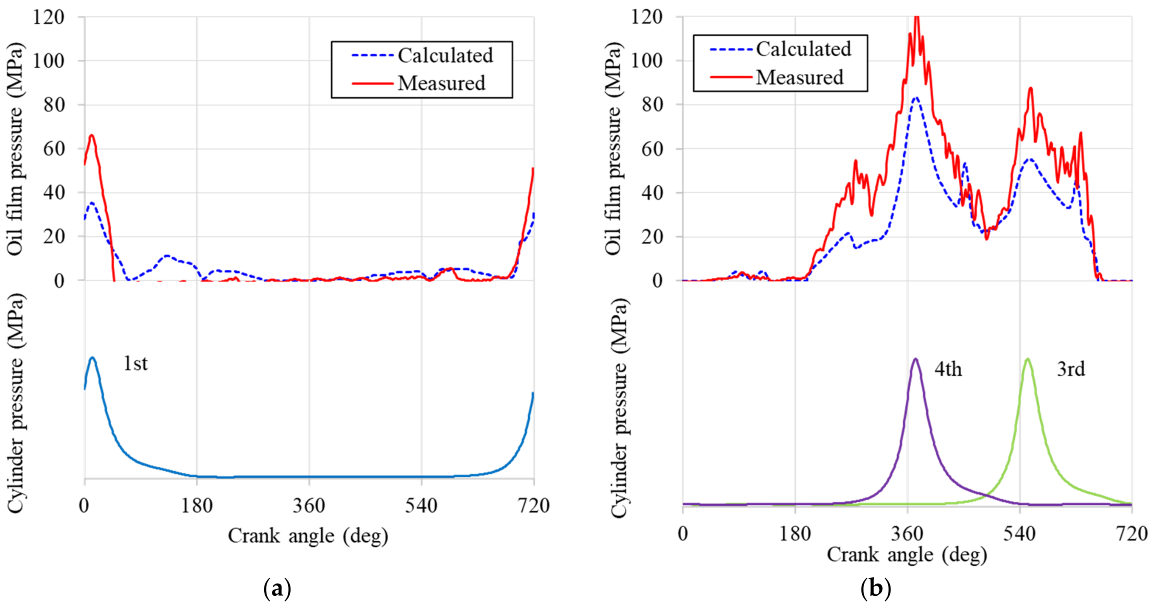

Figure 18. Measured and calculated oil film pressures (5000 rpm, full load: (**a**) oil film pressures at ♯1-R; (**b**) oil film pressures at ♯4-R.

Figure 19 compares the measured and calculated results when the load was full and the engine speed was 13,000 rpm. Figure 19a shows the oil film pressure of journal #1-R. The oil film pressure increased around 10 degrees of crank angle due to the increase in cylinder pressure in the 1st cylinder. In addition, an increase in oil film pressure was also measured near the bottom dead center of 180 degrees and 540 degrees, and these are thought to be due to the downward inertial force of the piston of the 1st cylinder near the bottom dead center in the high rotation region of 13,000 rpm. Comparing the measured results with the calculated results, it can be seen that the oil film pressure peaked at almost the same crank angle for both. At a crank angle of 10 degrees, the measured and calculated maximum pressures were 68 MPa and 27 MPa, respectively, with the calculated value approximately 60% lower than the measured value.

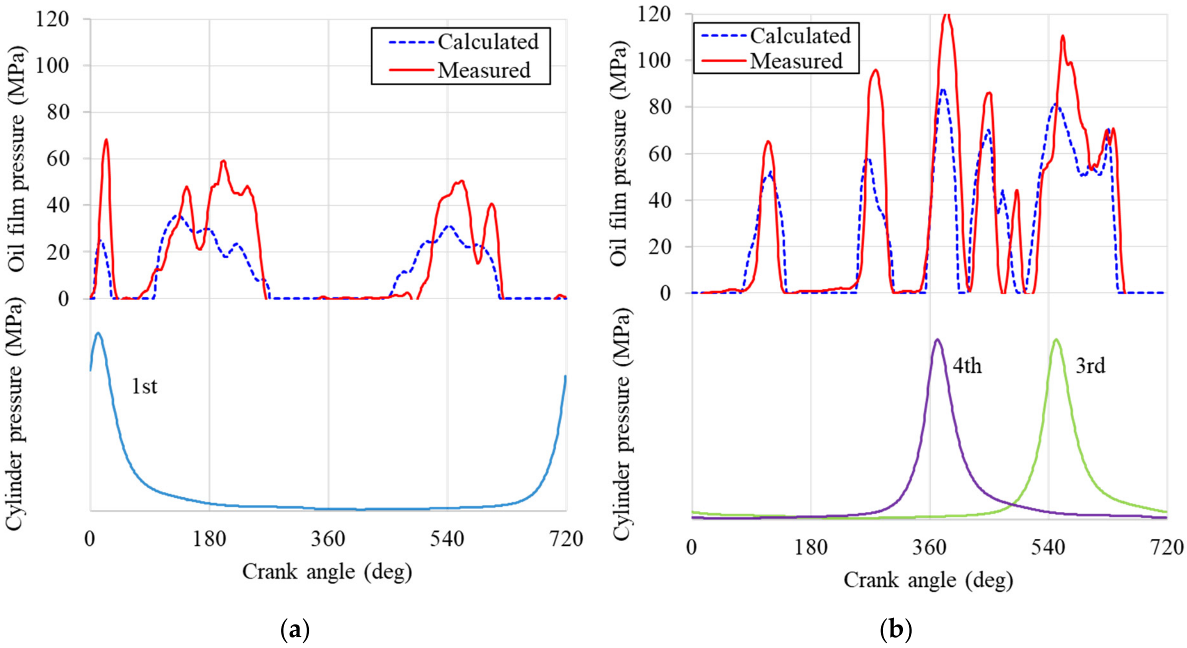

Figure 19. Measured and calculated oil film pressures (13,000 rpm, full load): (**a**) oil film pressures at ♯1-R; (**b**) oil film pressures at ♯4-R.

Figure 19b shows the experimental and calculated results of the oil film pressure at #4-R. The oil film pressure increased at crank angles of 375 degrees and 555 degrees due to the bearing load caused by the internal pressure of the 4th cylinder. On the other hand, oil film pressure peaks also occurred at crank angles of 90, 270, 450, and 630 degrees.

These factors are due to the inertial force of the piston, similar to measurement point #1-R. However, unlike the #1-R, it occurred during the upward or downward stroke of the pistons of the 4th and 3rd cylinders. In other words, the 3rd and 4th cylinders adjacent to #4-R were out of phase by 180 degrees, and the inertial forces of the respective pistons cancelled each other out at the top dead center or the bottom dead center. However, this is because a downward bearing load was generated due to the synthesis of inertial force during the upward and downward strokes of the piston.

Comparing the experimental value and the analytical value, the crank angle at which the pressure peak occurs was almost the same, and experimental verification data capturing this phenomenon were obtained. On the other hand, the maximum value of the oil film pressure was different.

5.3. Simulation of Oil Film Pressure Taking into Account Bearing Temperature

The difference between experimental and calculated oil film pressure values (analysis of oil film pressure incorporating bearing temperature) was also investigated.

At each measurement point and experimental conditions of the sliding bearing shown in Figures 18 and 19, the calculated value of the oil film pressure was lower than the measured value. As a factor, it was considered that the clearance of the bearing initially set in the calculation was different due to the temperature rise in the bearing experiment. Therefore, an analysis was performed by calculating the change in bearing clearance using the actually measured bearing temperature. Figure 20 shows a comparison between the experimental results and analysis results for #4-R at a crankshaft speed of 13,000 rpm and full load. To compare the peak around the 400 deg crank angle, an experimental value of the bearing temperature was introduced into the calculation which increased the oil film pressure from 88 MPa before consideration to 97 MPa. Moreover, in the verification of other conditions, the analytical value of the oil film pressure increased and tended to approach the measured value. At other measurement points, the oil film pressure increased and tended to approach the experimental value. These results confirm that EHL analysis can accurately predict the timing of oil film pressure generation in the main bearing. In addition, the relative magnitude of each oil film pressure peak was consistent, and it is assumed that the dynamic behavior of the crankshaft due to the combustion load and inertial load can be reproduced. The absolute value of the oil film pressure was generally lower than the experimental value, but it achieved the measured value by considering the bearing clearance during a bearing temperature increase. In addition, we believe that more accurate calculations are possible by reproducing accurate bearing clearances in consideration of bearing deformation and thermal deformation distribution due to bolt tightening.

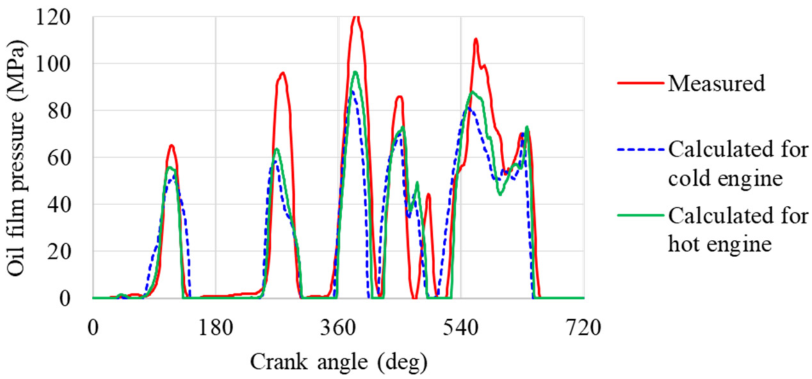

Figure 20. Oil film pressures due to bearing clearance differences between cold and hot engine conditions.

6. Conclusions

Using a newly developed highly durable thin-film sensor, we measured the oil film pressure distribution of the main bearing at 13,000 rpm of a high-speed high-power motorcycle engine, which had not been measured before.

1. In order to improve the accuracy of predicting the oil film pressure distribution using the analysis model, the shape of the main bearing after engine break-in was used as the standard. This shape was introduced into the analysis model as the initial shape, and the thin-film sensor was also formed along this shape.
2. A diamond-like carbon film with a thickness of 2 μm was applied to the protective film to improve the durability of the thin-film sensor under high-rotation and high-load operation conditions. As a result, the oil film pressure values at nine locations on five main bearings could be simultaneously measured with a four-cylinder engine.
3. When the engine load was changed in the experiment, there was little change in the maximum oil film pressure due to the difference in load for all five main bearings at the measurement position just below the shaft. In addition, main bearings #2 and #4, possessing a small sliding area and high surface pressure, had a higher oil film pressure than the other bearings, exceeding a maximum value of 140 MPa.

4. The increase in oil film pressure was measured in all main bearings from the results of experiments with varying rotational speeds at full load. In particular, the #3 and #5 main bearings tended to increase the oil film pressure due to the increase in inertial force as the rotational speed increased. As a feature of the experiment where the rotational speed was increased, since the main bearing was affected by the downward inertial force acting on each bearing, oil film pressure corresponding to the rotational speed was generated at crank angles other than the cylinder pressure adjacent to each main bearing. This study highlights this phenomenon, especially at the measurement point of the ♯1 main bearing.
5. The calculation results obtained by the analysis software (AVL/EXCITE) were compared with the actual measurement results and verified. The crank angle at which maximum film pressure occurred was the same for both results. Therefore, it was assumed that the simulation model accurately reproduced the dynamic crankshaft behavior caused by combustion and inertial loads. On the other hand, it was found that the difference in oil film pressure values between the calculation and the experiment was about 30 to 60%, and the experimental value was generally higher.
6. Regarding the difference in oil film pressure value, the temperature of the engine bearing was introduced into the analysis model. As a result, the analysis result was closer to the measured value. We found that a change in bearing clearance due to thermal expansion was actually achieved. As a further improvement, it is believed that a more accurate simulation model can be constructed by considering thermal deformation due to temperature distribution and bearing deformation due to the bolt-tightening torque.

Author Contributions: Conceptualization, Y.M. and Y.N.; methodology, Y.M. and M.O. (Michiyasu Owashi); formal analysis, S.K.; investigation, M.O. (Michiyasu Owashi) and Y.K.; resources, K.I.; data curation, T.I., M.O. (Michiyasu Owashi), and Y.K.; writing—original draft preparation, T.I.; writing—review and editing, M.O. (Michiyasu Owashi), M.O. (Masakuni Oikawa), Y.M., K.I., Y.K., S.K., and Y.N.; visualization, T.I., M.O. (Michiyasu Owashi), and Y.K.; supervision, M.O. (Michiyasu Owashi), M.O. (Masakuni Oikawa), Y.M. and Y.N.; project administration, Y.M. and K.I. All authors have read and agreed to the published version of the manuscript.

Funding: This research received no external funding.

Data Availability Statement: Not applicable.

Conflicts of Interest: M.O. was employed by the company Sustainable Engine Research Center Co. Ltd.. The remaining authors declare that the research was conducted in the absence of any commercial or financial relationships that could be construed as a potential conflict of interest.

References

1. Kawase, T.; Someya, T. Investigation into the oil film pressure distribution in dynamically loaded journal bearings. *Trans. Jpn. Soc. Mech. Eng. Ser. C* **1985**, *51*, 2562–2570. [CrossRef]
2. Masuda, T. A Measurement of Oil-film Pressure Distribution in Connecting Rod Bearing With Rest Rig. *Tribol. Trans.* **1985**, *35*, 71–76. [CrossRef]
3. Natsumeda, T.; Someya, T. Negative pressures in statically and dynamically loaded journal bearings. *Tribol. Ser.* **1986**, *11*, 65–72.
4. Bridgeman, P.W. *The Physics of High Pressure*; George Bell & Sons: London, UK, 1931; Chapter VII.
5. Kannel, J.W.; Bell, J.C.; Allen, C.M. Methods for Determining Pressure Distribution in Lubricating Rolling Contact. *ASLE Trans.* **1965**, *8*, 250–270. [CrossRef]
6. Köhler, A. Die Entwicklung von Aufgedampften Messwertaufnehmern und Deren Anwendung zur Druck-und Temperaturmessung in Geschmierten Wältz-und Gleitkontakten. Ph.D. Thesis, Technische Hochschule Aachen, Aachen, Germany, 1981.
7. Mihara, Y.; Someya, T. Measurement of Oil-Film Pressure in Engine Bearings Using a Thin-Film Sensor. *Tribol. Trans.* **2002**, *45*, 11–20. [CrossRef]
8. Inui, M.; Kobayashi, M.; Oowaki, K.; Furukawa, T.; Mihara, Y.; Owashi, M. Analysis of Oil Film Generation on the Main Journal Bearing Using a Thin-Film Sensor and Elasto-Hydrodynamic Lubrication (EHL) Model. *SAE Int.* **2003**, *6*, 119–125. [CrossRef]

9. Miura, K.; Owashi, M.; Mihara, Y. High Durability Thin-Film Pressure Sensor Development. In Proceedings of the Ninth International Conference on Modeling and Diagnostics for Advanced Engine Systems (COMODIA 2017), C314, Okayama, Japan, 25–28 July 2017.
10. Kamiya, M.; Kobayashi, T.; Mihara, Y.; Someya, T. Measurement of Piston Skirt Oil-film Pressure under Piston Slap. *SAE Trans.* **2007**, *116*, 1654–1659.
11. Miura, K.; Kobayashi, K.; Yamakawa, N.; Saruwatari, M.; Mihara, Y. Measurement of Oil Film Pressure in Piston Pin-Boss by Thin-Film Pressure Sensor. In Proceedings of the SAE 2015 Powertrains, Fuels & Lubricants International Meeting, Power Train Tribology 2015, Kyoto, Japan, 1–4 September 2015. 01-2040.
12. Miura, K.; Owashi, M.; Mihara, Y. Thin Film Sensors for Measuring Oil Film Condition in Engine Sliding Surfaces. In Proceedings of the World Tribology Congress 2017, Oral Presentation, Beijing, China, 17–22 September 2017.
13. Mochizuki, K.; Watanabe, Y.; Owashi, M.; Mihara, Y. A Study on Sliding Surface Pressure Measurement of Piston Ring under Reciprocating Condition Using Thin-film Sensor. *Tribol. Online* **2019**, *14*, 179–187. [CrossRef]
14. Ebner, M.; Ziegltrum, A.; Lohner, T.; Michaelis, K.; Stahl, K. Measurement of EHL temperature by thin film sensors—Thermal insulation effects. *Tribol. Int.* **2020**, *149*, 105515. [CrossRef]
15. Hofmann, S.; Yilmaz, M.; Maier, E.; Lohner, T.; Stahl, K. Friction and contact temperature in dry rolling-sliding contacts with MoS2-bonded and a-C:H:Zr DLC coatings. *Int. J. Mech. Mater. Eng.* **2021**, *16*, 16. [CrossRef]
16. Ono, Y.; Matsumoto, K.; Mihara, Y. A Study of the Lubrication under Impact Loading—Experimental and Analytical Application to Push Belt CVTs *Tribol. Online* **2019**, *14*, 18–23. [CrossRef]
17. Kano, M. Diamond-Like Carbon Coating Applied to Automotive Engine Components. *Tribol. Online* **2014**, *9*, 135–142. [CrossRef]
18. Iwata, T.; Oikawa, M.; Chida, R.; Ishii, D.; Ogihara, H.; Mihara, Y.; Kano, M. Excellent Seizure and Friction Properties Achieved with a Combination of an a-C:H:Si DLC-Coated Journal and an Aluminum Alloy Plain Bearing. *Coatings* **2021**, *11*, 1055. [CrossRef]
19. Iwata, T.; Owashi, M.; Oikawa, M.; Mihara, Y.; Kobayashi, K.; Yamakawa, N. Measurement of Piston Pin-Bore Oil Film Pressure under Engine Operation. *Lubricants* **2022**, *10*, 258. [CrossRef]
20. Mabuchi, Y.; Higuchi, T.; Inagaki, Y.; Kousaka, H.; Umehara, N. Wear analysis of hydrogen-free diamond-like carbon coatings under a lubricated condition. *Wear* **2013**, *298–299*, 48–56. [CrossRef]
21. Horiuchi, T.; Kano, M.; Yoshida, K.; Kumagai, M.; Suzuki, T. Method of Applying DLC Coating on Aluminum Alloys. *Tribol. Online* **2010**, *5*, 136–143. [CrossRef]
22. Ronkainen, H.; Varjus, S.; Holmberg, K. Friction and wear properties in dry, water- and oil-lubricated DLC against alumina and DLC against steel contacts. *Wear* **1998**, *222*, 120–128. [CrossRef]